ACS APPLIED MATERIALS & INTERFACES

Research Article

www.acsami.org

Directed Assembly of Bifunctional Silica–Iron Oxide Nanocomposite with Open Shell Structure

Hui Xin Che,[†] Swee Pin Yeap,[†] Mohamed Syazwan Osman,[†,‡] Abdul Latif Ahmad,[†] and JitKang Lim*[,†,§]

[†]School of Chemical Engineering, Universiti Sains Malaysia, 14300 Nibong Tebal, Penang, Malaysia

[‡]Faculty of Chemical Engineering, Universiti Teknologi MARA, 13500, Permatang Pauh, Pulau Pinang Malaysia

[§]Department of Physics, Carnegie Mellon University, Pittsburgh, Pennsylvania 15213, United States

Supporting Information

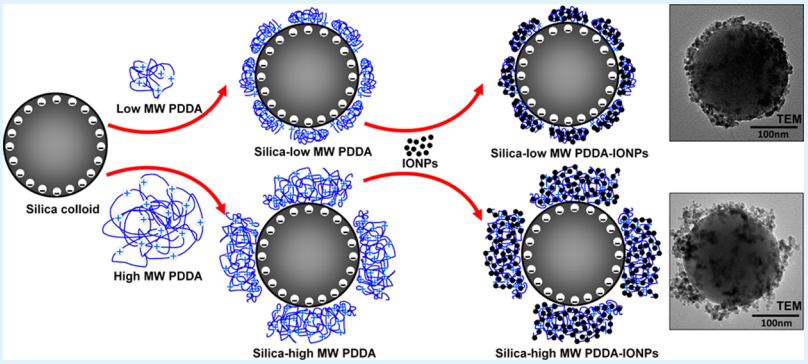

ABSTRACT: The synthesis of nanocomposite with controlled surface morphology plays a key role for pollutant removal from aqueous environments. The influence of the molecular size of the polyelectrolyte in synthesizing silica–iron oxide core–shell nanocomposite with open shell structure was investigated by using dynamic light scattering, atomic force microscopy, and quartz crystal microbalance with dissipation (QCM-D). Here, poly(diallydimethylammonium chloride) (PDDA) was used to promote the attachment of iron oxide nanoparticles (IONPs) onto the silica surface to assemble a nanocomposite with magnetic and catalytic bifunctionality. High molecular weight PDDA tended to adsorb on silica colloid, forming a more extended conformation layer than low molecular weight PDDA. Subsequent attachment of IONPs onto this extended PDDA layer was more randomly distributed, forming isolated islands with open space between them. By taking amoxicillin, an antibiotic commonly found in pharmaceutical waste, as the model system, better removal was observed for silica–iron oxide nanocomposite with a more extended open shell structure.

KEYWORDS: *nanocomposite, silica colloid, iron oxide nanoparticles, open shell structure, amoxicillin degradation*

1. INTRODUCTION

Nanoparticles are one of the most prominent and promising candidates under active pursue for environmental engineering application. For water treatment purposes, achieving high colloidal stability is always the main concern.[1,2] In this regard, self-assembly of nanoparticles[3] has been proposed as one of the important processes toward minimizing aggregation and flocculation. Through this approach the building blocks, which are composed of both nanoparticles and other constituent materials, can be assembled into an ordered structure via either direct or indirect interaction in a highly controllable manner.[4] Guiding assembly of nanoparticles with high precision can ensure the construction of the desired morphology at nanoscale for various applications.[5,6] For instance, Liz-Marzan's group reported that well-defined mono- and multilayers of carbon nanotubes can be deposited on various spherical colloids by using layer-by-layer assembly.[7] In their work, the concept of directed-assembly is applied since it is a powerful strategy to assemble the building blocks into an ordered and desired architecture.[8] Hence, by designing particles with stimuli responsive interparticle interaction, well-defined magnetic core–shell particle can be organized into ordered structure due to the guided interaction.

In agreement with the definition of directed-assembly, a polycation such as poly(diallydimethylammonium chloride) (PDDA) serves as a bridging agent, permitting iron oxide nanoparticles (IONPs) to be attached onto the like-charged silica colloid template for triggering guided assembly via straightforward electrostatic interactions. From the chemical point of view, this implies that PDDA plays a role as a bridging agent to control the localization of IONPs onto the colloidal surface.[9] In terms of a geometrical view, the PDDA adlayer acts as a scaffold for IONPs to be arranged onto a precoated silica template, forming core–shell morphology with fractal

Received: March 13, 2014
Accepted: September 8, 2014
Published: September 8, 2014

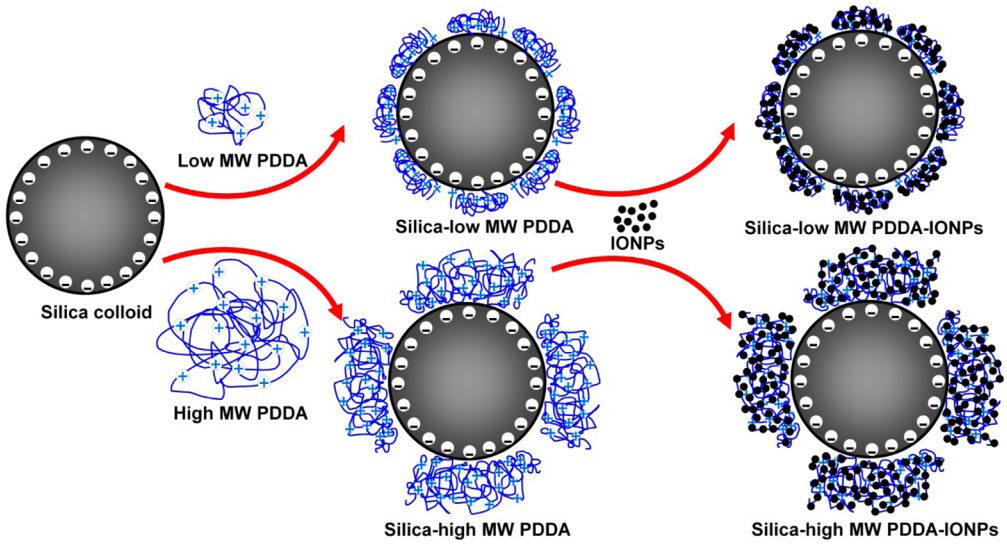

Figure 1. Schematic diagram showing the major steps involved in directed-assembly of silica–PDDA–IONPs nanocomposite. Negatively charged silica colloid is surface functionalized with cationic polyelectrolyte PDDA first and later subjected to the attachment of negatively charged IONPs. Low MW PDDA forms a more compact polyelectrolyte layer, and high MW PDDA tends to form a more extended layer.

structure.[10] In a nutshell, the directed assembly of core–shell nanoparticles with magnetic and catalytic properties can be developed with a versatile technique by relying on surface charge reversal of the building blocks employed.

By combining silica colloids, polycationic PDDA, and IONPs into one unified nanostructure with core–shell morphology would allow the end users to take full advantage of the unique properties of each constituent materials.[11] It is important to mention that silica colloids play a key role as an anchoring platform for the attachment of flexible polyelectrolyte, which further allows the incorporation of IONPs. In fact, the inert mesoporous silica colloids are surface-modifiable, so the adsorption of other species of nanomaterials can be carried out easily.[12] Attachment of IONPs onto the highly colloidal, stable silica colloids not only could prevent the self-agglomeration of magnetic nanoparticles in solution but at the same time maintain their high surface area-to-volume ratio.[13] Moreover, the confinement of IONPs onto the polyelectrolyte-modified silica colloid reduces the direct exposure of bare IONPs to environment, where the small dimension of IONPs tends to induce nanotoxicity.[14,15] Furthermore, the polyelectrolyte network that surround the silica colloids, forming an open matrix, provides an additional capture zone to accommodate incoming targeted pollutant from the aqueous environment. In general, due to the cooperative nature of the magnetophoresis,[16,17] silica–PDDA–IONPs core–shell structure not only embraces the catalytic property of bare IONPs but at the same time enhances the magnetophoretic separation rate compared to that of bare IONPs.[18,19]

In particular, polymer is widely exploited as an attractive building block in fabricating hybrid composites such as cellulose nanocrystals[20] and nanotubes.[21] Considerable efforts have been made in recent years to pursue composite materials of different morphologies and explore their application.[22] Altering polymer molar mass can be one of the strategies in constructing complex polyelectrolyte layers and multicomposite films with open shell structure that is suitable for environmental engineering applications.[23,24] We hypothesized that the incorporation of IONPs into this open shell structure would greatly enhance the pollutant removal capability of silica–PDDA–IONPs core–shell nanocomposite. The degree of voidness of this open structure, after the incorporation of IONPs, can be adjusted through the use of polyelectrolyte with different molecular weight. However, to the best of our knowledge, the study of directed-assembly silica–IONPs core–shell nanoparticle with open shell matrix driven by the attachment of polyelectrolyte with different molecular weight is not well-established. Thus, questions concerning the role of conformation change of polyelectrolyte in dictating the shell structure still need to be further investigated. It is the purpose of this study to synthesize silica–PDDA–IONPs nanocomposite with open shell morphology and to demonstrate its feasibility for environmental engineering applications.

The work described herein was intended to introduce an approach toward fabricating controlled surface morphology of magnetic core–shell nanoparticles via different polyelectrolyte molecular weight and to explore the impacts of the as-synthesized nanocomposite for water treatment purposes. In order to define and investigate the development of silica–PDDA–IONPs nanocomposite, a comprehensive set of characterization techniques are explored. For instance, the evolution of the silica–PDDA–IONPs nanocomposite, from its building blocks, is monitored and characterized using dynamic light scattering (DLS) (Malvern Instruments, Zetasizer Nano-ZS) and quartz crystal microbalance with dissipation (QCM-D) (Q-Sense E1, Sweden). Transmission electron microscopy (TEM) (JEOL, JEM-20CX) and atomic force microscopy (AFM) (Park System, XE-100) are used in conjunction to further explore the surface properties of the nanocomposite formed. Last, but not least, the possible leaching of iron from the synthesized nanocomposite is analyzed by inductively coupled plasma-optical emission spectrometry (ICP-OES) (PerkinElmer Optima 7300 DV with autosampler model S10).

There has been very little to almost no evaluation of engineering usage related to the different surface morphology accounting for variation in the open shell structure. In this study, we employed the antibiotic amoxicillin (AMX) as the model system to test our hypothesis. AMX is a broad-spectrum β-lactam antibiotic that belongs to the penicillin group, which is

Table 1. Hydrodynamic Diameter with Polydispersity Index (PDI) for All of the Building Blocks and Nanocomposite As Measured by DLS and Their Associated Electrophoretic Mobility and ζ-Potential[a]

system	component	hydrodynamic diameter (nm)	PDI	ζ-potential (mV)	electrophoretic mobility (μm cm/V s)
1	silica	234.7	0.025	−57.0	−4.460
	low MW PDDA	96.7	0.909	+34.4	+2.695
	silica−low MW PDDA	255.3	0.041	+51.0	+3.989
	IONPs	62.2	0.151	−16.4	−1.284
	silica−low MW PDDA−IONPs	352.1	0.307	+28.2	+2.208
2	silica	234.7	0.025	−57.0	−4.460
	high MW PDDA	193.5	0.966	+44.1	+3.460
	silica−high MW PDDA	299.2	0.083	+56.6	+4.423
	IONPs	62.2	0.151	−16.4	−1.284
	silica−high MW PDDA−IONPs	440.8	0.411	+29.4	+2.310
3	AMX	0.8[b]	0.981	+0.578	+0.045

[a]All measurements were made with a Malvern Instruments Zetasizer Nano-ZS. The solution pH was in the range of 6.3−6.8. [b]The size of amoxicillin is reported as an averaged number and is different from other values, which are reported as average intensity. The purpose of this variation is to enable the direct comparison of amoxicillin size to the existing value (reported as 1.3 nm) in the literature.[34]

generally used in veterinary medicine as well as human prescription medicine.[25] Toxic effects of the AMX remaining in wastewater toward algae and aquatic microorganisms are massively reported.[26,27] Therefore, considerable effort has to be allotted for removing AMX from the environment. By taking AMX as our modeled system, the capability of open shell silica−PDDA−IONPs nanocomposite for pollutant removal can be tested.

2. MATERIALS AND METHODS

2.1. Materials. All the reagents utilized in this work were of analytical grade and used as received without further purification. Ethanol (absolute), sodium hydroxide (NaOH), and hydrogen peroxide (H_2O_2, 100 volumes >30%w/v) were bought from Fisher Scientific (M) Sdn. Bhd. Ammonia solution (25%) was supplied by Merck. Poly(diallydimethylammonium chloride) (PDDA) with the low molecular weight of 100 000−200 000 and high molecular weight of 400 000−500 000 were provided by Aldrich Chemistry. Tetraethylorthosilicate (TEOS, 98%), magnesium chloride ($MgCl_2$), iron(III) chloride ($FeCl_3$, 98% pure, anhydrous), and iron(II) chloride ($FeCl_2 \cdot 4H_2O$, 99%) were obtained from Acros Organics. Amoxicillin trihydrate and sodium dodecyl sulfate, approximately 95% based on total alkyl sulfate content, were purchased from Sigma-Aldrich. In all experiments, Milli-Q water was employed from PureLab Option-Q with resistivity at 18 MΩ·cm from a potable water source.

2.2. Preparation of Silica−PDDA−IONPs. The pictorial representation of silica−PDDA−IONPs nanocomposite synthesis is shown in Figure 1. The procedure described here was implemented for the development of silica−PDDA−IONPs nanocomposite by using either low or high molecular weight PDDA as the intermediate layer, where the detailed preparation methods can be found in our previous publication.[18] Submicron-sized, monodispersed silica colloids were synthesized via the Stöber process by mixing ethanol, TEOS, and ammonia in a volume ratio of 30:1:3 and magnetically stirring at 500 rpm for 2 h.[28] The synthesized silica colloids were then subjected to three cycles of washing before PDDA attachment. In the subsequent step, these silica colloids were surface-functionalized by cationic PDDA with mass ratio of 1:8 in order to promote full coverage of silica colloids with PDDA. It is worthwhile to note that the PDDA was introduced at 500 times in excess of the estimated amount needed to form a monolayer in order to ensure full coverage of the silica surface with PDDA molecules. The formation of this cationic PDDA layer on silica colloids would promote the subsequent attachment of the negatively charged IONPs, leading to the formation of a nanocomposite with a silica core and IONPs shell as the final structure.

As IONPs synthesis, we used a coprecipitation method with the ferric (Fe^{3+}) and ferrous (Fe^{2+}) ratio at 2:1.[29] In short, the ferric chloride and ferrous chloride powders were mixed in deareted Milli-Q water before being heated to reflux while being stirred with a magnetic stirrer. Once the temperature of the reaction mixture reached 70 °C, 2.5 M NaOH was added, and the reaction continued stirring magnetically for another 30 min before the black precipitate was collected using a permanent magnet. This reaction is carried out under continuous aeration with argon gas. Lastly, the ratio of added IONPs to polyelectrolyte-functionalized silica colloids surface area was maintained at around 126 mg/m^2 for the final construction of silica−PDDA−IONPs nanocomposite, regardless of which PDDA was used (either low or high). Hence, the absolute amount of IONPS available in either suspension to carry out the function as catalyst is roughly equal. All of the solutions of the synthesized nanoparticles were prepared in a final concentration of 0.01 g/mL for further usage.

In our study, all the electrophoretic mobility measurements were conducted with a Malvern Zetasizer Nano-ZS series. Later, we calculated the ζ-potentials of all nanoparticles/nanocomposite we synthesized upon the basis of the Helmholtz−Smoluchowski approximation. This approach is more universal and straightforward for the ease of comparison among the nanomaterials we synthesized with different surface morphology. For a more realistic approximation of the ζ-potential exhibited by a hairy nanostructure, such as silica−PDDA and/or silica−PDDA−IONPs nanocomposite, we refer the readers to Ohshima's soft particle approximation.[30] There is no pH control during the DLS and zeta potential measurements in which all the background solutions are 0.1 mM NaCl with pH at around 6.3−6.8.

Since the attachment of subsequent components onto the silica colloid is mainly driven by electrostatic interaction, the detected ζ-potential changes from silica colloid to silica−PDDA and finally silica−PDDA−IONPs confirmed the successful formation of the final core−shell structure from its building blocks (as shown in Figure 1). Both results on ζ-potential and electrophoretic mobility of nanomaterials at each stage of synthesis are summarized in Table 1. Freshly synthesized silica colloids, by using the Stöber process, were initially negatively charged with a ζ-potential at −57.0 mV. The addition and attachment of low or high molecular weight PDDA (as binding agents) on silica colloids were accompanied by surface charge reversal with detected ζ-potential at +51.0 and +56.6 mV, respectively. This inversion of surface charge could serve as the best evidence that PDDA charge had completely overcompensated the silica anion. Further exposure of IONPs to these PDDA-decorated silica colloids would lead to the formation of silica−PDDA−IONPs nanocomposite due to the attachment of negatively charged IONPs. The final structure of silica−PDDA−IONPs, constructed with either low or high molecular weight PDDA as binding agent, was positively charged with net ζ-potential at +28.2 and +29.4 mV, respectively. These results elucidated that the immobilization of IONPs into the regime of silica−PDDA had suppressed the highly positively charge PDDA layer. In fact, the excess

of polyelectrolyte charge is believed to provide extra stabilization for the nanocomposite formed.

In addition, TEM micrographs shown in Figure 2 revealed the surface morphology of the nanoparticles synthesized at each stage and

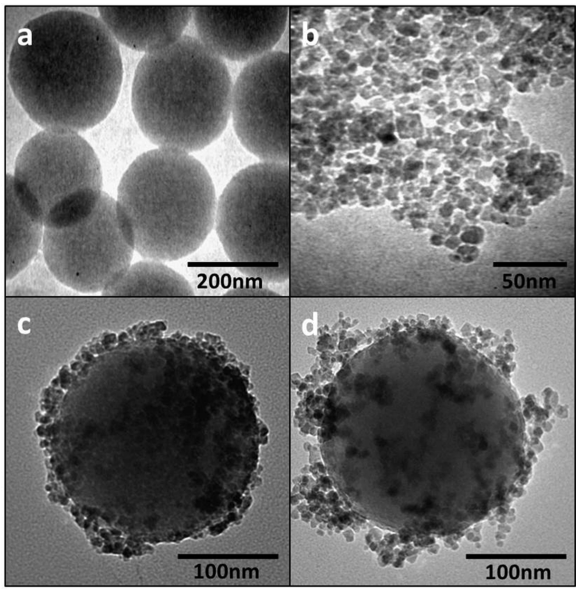

Figure 2. TEM micrographs of (a) silica colloids, (b) IONPs, (c) silica−low MW PDDA−IONPs, and (d) silica−high MW PDDA−IONPs.

also confirmed the successful fabrication of the nanoparticles. The sizes of silica colloids, IONPs, silica−low MW PDDA−IONPs and silica−high MW PDDA−IONPs determined from TEM and DLS analysis are compared and tabulated in Table S1 in the Supporting Information. There is good agreement for the size of silica colloids in terms of 228.0 ± 1.9 nm measured by TEM and 234.7 ± 0.7 nm measured by DLS. However, the hydrodynamic size analyzed by DLS of IONPs, silica−low MW PDDA−IONPs, and silica−high MW PDDA was apparently greater than the actual size denoted by TEM (see Table S1 in Supporting Information). In this case, the interpretation of DLS data may involve the interplay of various factors, such as electroviscosity, surface roughness, and shape irregularity, which are believed to be responsible for the large size differences between DLS and TEM.[31] Besides, the particle shrinkage due to sample drying for electron microscopy imaging may contribute to the small particle size observed by TEM compared to DLS.

Apart from that, the colloidal stability of the synthesized IONPs and silica−PDDA−IONPs nanocomposite was monitored across the averaged hydrodynamic diameter over a time course of 500 min using DLS. The concentration of the analyzed solutions was 10 ppm. The recorded average hydrodynamic diameter of the respective synthesized nanoparticles was maintained at a certain range, depicting the good colloidal stability of the as-synthesized nanoparticles in suspension (see Figure S1 in the Supporting Information). We anticipated that the size mismatch between the IONPs and silica colloid[32] and the colloidal stability of both nanomaterials are the determining factors for the successful formation of a well-defined core−shell structure. Besides, the magnetophoretic response of synthesized IONPs as well as silica−PDDA−IONPs nanocomposite (either low or high MW PDDA) was examined in terms of the suspension opacity rate under the influence of a NdBFe cylindrical magnet. Figure S2 in the Supporting Information demonstrated that both silica−PDDA−IONPs are more magnetically responsive than IONPs.[18] In addition, time lapse images in Figure S3 of the Supporting Information are the best illustration showing the superior magnetic collectability of nanocomposite compared to bare IONPs. This improvement in magnetic response compared to that of bare IONPs is attributed to the cooperative nature of magnetophoresis.[9,17] Furthermore, this nanocomposite also experienced much lesser thermal randomization energy but greater magnetophoretic force compared to individual IONPs.[18] All these factors contribute to a high magnetic separation rate with reduced collection time of the synthesized nanocomposite, which qualified it as a good candidate for on-site water treatment applications.[33]

2.3. Preparation of Bilayers with QCM-D. The PDDA polyelectrolyte solution was prepared at a concentration of 0.009 g/mL. For QCM-D measurement, the IONPs solution was diluted to 1 × 10^{-5} g/mL. The AT-cut piezoelectric quartz crystal coated with thin silica electrodes was first cleaned in a 2% (w/v) sodium dodecyl sulfate (SDS) solution for 30 min, rinsed under a stream of running Milli-Q water, and then blow-dried with nitrogen gas before mounted with extra care into the cleaned flow cell. The flow cell was also thoroughly rinsed with 2% SDS and Milli-Q water before placing it into the chamber holder. The working solutions were degassed through ultrasonication for 10 min and stored in a water bath at 27 °C, which is exactly 2 °C above the experimental temperature, before use. In addition, the adsorption solution was prepared on a weekly basis. The measurement was begun with the injection of Milli-Q water through the silica-coated quartz crystal until a steady baseline was achieved. The PDDA and IONPs solution was consecutively introduced into the system at a constant flow rate of 20 μL/min to monitor their adsorption behavior. After PDDA adsorption was complete, an excess of nonadsorbed or loosely bound PDDA was first removed by rinsing with Milli-Q water before switching to IONPs solution. A similar step was conducted for either low or high molecular weight PDDA solution when constructing the first layer on the silica-coated quartz crystal. The response of frequency and dissipation factor of the crystal sensor, corresponding to the deposition of PDDA and IONPs, was monitored at *n*th harmonics (n = 1, 3, 5, 7, 9). In our QCM-D experiment, the ratio of dissipation shift to frequency shift was considerably large (see the discussion below). This feature accounted for the viscoelastic property reported in the studies of protein and DNA films.[35,36] Hence, theoretical analysis of the collected data is carried out by using a Voigt-based model. The Sauerbrey relation is invalid here to deduce the effective thickness of the viscoelastic film on the crystal surface.

2.4. Amoxicillin Removal Test. The reaction mixture, composed of AMX and tested silica−PDDA−IONPs, was left on an end-to-end rotating mixer with rotational speed at 40 rpm for 6 days to achieve the highest possible removal efficiency for comparison between silica−PDDA and silica−PDDA−IONPs of concentration 0.01 g/mL. After the reaction period, the nonmagnetic silica−PDDA nanoparticles were separated out from the suspension by using centrifugation at 10 000*g*. Silica−PDDA−IONPs nanocomposite, on the other hand, was separated out from the supernatant by using a neodymium boron ferrite (NdBFe) cylindrical magnet with a surface magnetization at ∼6000 G (Ningbo YuXiang E&M Int'l Co., Ltd.). For the removal test, 20 ppm of AMX was used as the initial concentration, and the subsequent changing of AMX concentration in supernatant upon completion of each experiment was monitored by UV−vis spectrophotometer (Agilent Technologies, Cary-60) at a maximum wavelength of 274 nm.[37] In all these AMX removal experiments, deionized water was employed as background medium with pH 6.3−6.8, and no further pH adjustment was performed. It is worth mentioning that there are altogether 16 intermediates could be generated as AMX degrades under the Fenton reaction, as discussed by Trovó and co-workers.[38] According to their study, there are three possible pathways for AMX degradation, mainly involving the opening of the β-lactam ring, decarboxylation, hydroxylation of the benzoic ring, and several other oxidation steps.[38] In fact, the major AMX degradation byproduct was identified as AMX-penicilloic acid produced through the opening of the β-lactam ring via hydrolysis, which was then transformed to AMX-penilloic acid after the decarboxylation process.[39,40] Therefore, we monitored the temporal concentration changes of AMX at its maximum absorbance wavelength of 274 nm to minimize the interferences from other intermediate compounds.

Table 2. Film Thickness Increment for Different Combinations of PDDA Molecular Weight and IONPs with Respect to Silica

system	component	thickness increment (nm)	
		DLS	QCM-D
1	low MW PDDA–silica	10.3 ± 2.3	5.2 ± 0.5
	IONPs–low MW PDDA–silica	58.7 ± 27.3	42.6 ± 3.8
2	high MW PDDA–silica	32.3 ± 3.6	18.3 ± 3.1
	IONPs–high MW PDDA–silica	103.1 ± 40.1	80.6 ± 4.3

It is important to note that in our experiments with the presence of an oxidizing agent, H_2O_2, a mixture of AMX and H_2O_2 was used to make up the initial 20 ppm concentration as a control case. The control sample was prepared in such a way to offset the AMX removal efficiency contributed by the addition of H_2O_2, so that the difference in AMX removal efficiency is only influenced by the varying amount of nanomaterials suspension added into the system.

3. RESULTS AND DISCUSSION

3.1. Unique Features of Silica–PDDA–IONPs Nanocomposite. The evolution of silica–PDDA–IONPs size was monitored via DLS and QCM-D, and the measurement results are summarized in Table 2. Thickness of the low and high MW PDDA adlayer was recorded as 10.3 and 32.3 nm by DLS, as well as 5.2 and 18.3 nm by QCM-D. After the attachment of IONPs, the detected increment in layer thickness for silica–low MW PDDA–IONPs and silica–high MW PDDA–IONPs was 58.7 and 103.1 nm by DLS, as well as 42.6 and 80.6 nm by QCM-D. In general, these results show that the nanocomposite size increased with the deposition of each layer during the synthesis of core–shell particle by using different molecular weight PDDA as well as IONPs. In fact, a systematic thickness increment was observed in both systems by DLS and QCM-D measurements. However, in a very consistent manner (see Table 2), DLS always discovered a thicker adlayer compared to QCM-D, which is very likely due to the particles' curvature effect.[41] We do not expect complete agreement in both measurements, and this discrepancy in detected layer thickness is attributed to the different surface geometry for conducting the immobilization process.[42] Besides, adsorbate flowed through the flat silica-coated quartz crystal surface horizontally in QCM-D. The deposition adsorbates lead to charge overcompensation at the surface interface of the underlying layer. This in turn causes electrostatic repulsion and limits the adsorbates' adsorption to only one additional monolayer, where the excess adsorbates were removed by continuous flow of the subsequent adsorbates, resulting in a leveling (planarization) of the surface relief.[43] Conversely, DLS analyzed the hydrodynamic diameter of the as-synthesized nanoparticles suspended in bulk solution on an ensemble average, where a three dimensionally structured array condition is considered.[44] For this reason, thinner films of adsorbates spread on the silica-coated quartz crystal compared to films buildup in bulk solution. As a result, thickness increment values of constructed layers were smaller in QCM-D compared to DLS.

The adsorbed layer structure on the silica surface can be further investigated by QCM-D to evaluate its conformation after the adsorption. As for QCM-D measurement, both dissipation and frequency shift were commonly monitored simultaneously to extract the information about the viscoelasticity and the structural change of the adsorbed layer.[45] Figure 3a,b shows typical QCM-D measurements after the injection of PDDA and IONPs suspension. A decrease in frequency and an increase in dissipation were detected due to the particles

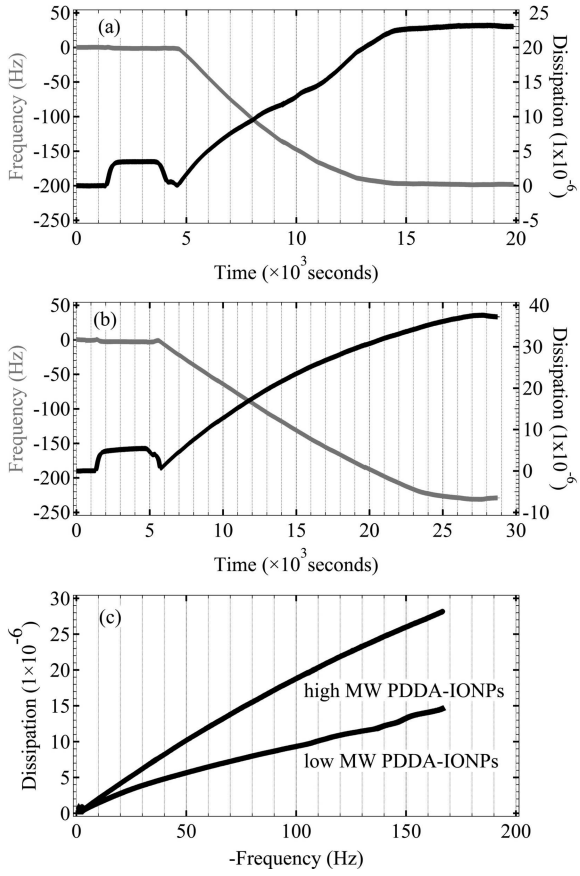

Figure 3. QCM-D measurement of frequency (gray line) and dissipation (black line) shift at the third overtone in the systems of (a) low MW PDDA and IONPs and (b) high MW PDDA and IONPs, as well as the (c) dissipation shift versus frequency shift using data from parts a and b.

deposition on the silica-coated quartz crystal surface. Frequency and dissipation shift generally showed different time dependencies. Thus, in order to relate the observed frequency and dissipation shift, a plot of changes in dissipation against changes in frequency (see Figure 3c) was constructed (hereafter known as D–f plot) to eliminate time-dependency as an explicit parameter. Direct inspection on the D–f plot recognized that the dissipation shift increased almost linearly with frequency shift. This linear behavior indicated that no conformational alteration occurred during the adsorption process on the surface.[46] In addition, as suggested by Höök and co-workers, a larger ratio of dissipation shift over frequency shift indicated the higher flexibility of the formed adsorption layer structure. This observation implied that the adsorbed film of high MW PDDA and IONPs (0.17×10^{-6} Hz^{-1}) was "softer" than the film of low MW PDDA and IONPs (0.087×10^{-6} Hz^{-1}).[36,47] All the above results have indirectly suggested the formation of more a extended open-shell structure for the case of high MW PDDA.

dx.doi.org/10.1021/am5050949 | ACS Appl. Mater. Interfaces 2014, 6, 16508–16518

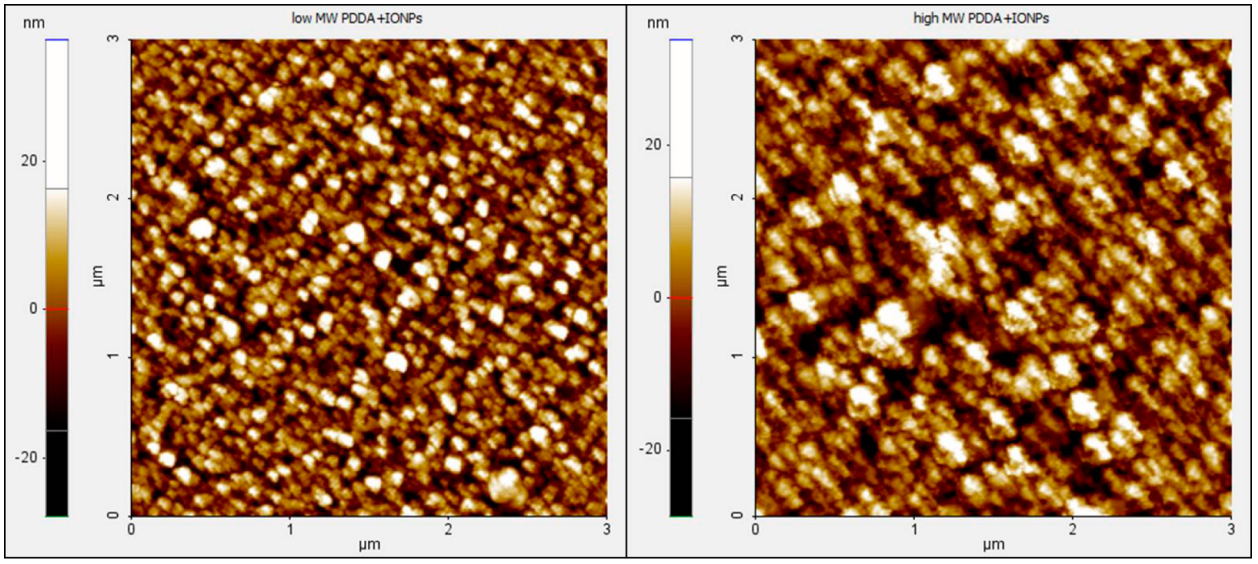

Figure 4. AFM images in 2D mode of the assembled films deposited on silica-coated quartz crystal in the systems of (left) low MW PDDA and IONPs and (right) high MW PDDA and IONPs.

After confirming the progressive increment of the thickness of the outer shell layers during the process of synthesizing silica–PDDA–IONPs through DLS and QCM-D analysis, AFM and TEM were further employed to provide topography information related to IONPs particle distribution on the silica colloid. AFM is a potent tool to characterize film surfaces at nanometer or subnanometer resolution,[48] where the localized conformation information on the bilayer buildup can be investigated. The top view of AFM shown in Figure 4a indicates densely packed IONPs with relatively good uniformity on the underlying PDDA film (low MW PDDA), with a root-mean square roughness of 5.5 nm (see Table 3). On the other hand, Figure 4b depicts incomplete surface coverage by IONPs, illustrating that the particles aggregated randomly on the bottom layer of PDDA (high MW PDDA), giving rise to a greater root-mean square roughness of 10.3 nm (see Table 3). This scattered distribution of particle islands is attributed to the strengthening of repulsive electrostatic interactions between the adsorbed high MW polyelectrolyte chains.[49] Furthermore, referring to TEM micrographs in Figure 2 shows that IONPs are more evenly distributed onto the regime of silica–low MW PDDA compared to silica–high MW PDDA. Moreover, particle clusters were found randomly formed on silica–high MW PDDA colloids. Hence, the two surface analyses of AFM and TEM consistently pointed out that the immobilization of IONPs onto silica colloid was more random, forming patchy surface morphology by using high MW PDDA as bridging agent.

Table 3. AFM Results of Root-Mean-Square Roughness (Rq, in nm) of Assembled Films on Silica-Coated Quartz Crystal

	low MW PDDA–IONPs	high MW PDDA–IONPs
Rq	5.528	10.268

3.2. Effect of Suspension Ionic Strength. Basically, PDDA with different molecular weight (MW) was attached to the silica colloids as bridging agent to promote the incorporation of IONPs. Hence, how well these PDDA layers extended out from the surface of the silica colloid should influence (1) the distribution of IONPs on the surface of the silica colloid and (2) the stretching of the PDDA network formed, which subsequently produce a void shell structure with a high degree of openness. Our TEM images serve as the best evidence to prove that the first hypothesis is valid. In order to verify the second hypothesis, we employed divalent salt $MgCl_2$ as background medium to vary the conformation of the PDDA layer of the synthesized nanocomposite based on a salting out effect. The structural change of PDDA during salt concentration adjustment, between 0 (in pure Milli-Q water) and 10 mM, is mostly the combined effect of entropy along with Coulomb interactions.[50] The averaged hydrodynamic diameter of silica–PDDA under the influence of suspension ionic strength was then monitored by using DLS. Figure 5 shows the percent decrement of the averaged hydrodynamic diameter of silica–PDDA as a function of the ionic strength. For instance, in pure Milli-Q water, the average hydrodynamic diameter of silica–low MW PDDA was 258.3 nm. By increasing the ionic strength to 4 mM $MgCl_2$, we observed 7.3% reduction in the hydrodynamic diameter of silica–low MW PDDA down to 239.2 nm. On the other hand, in salt-free solution, the averaged hydrodynamic diameter of silica–high MW PDDA was 328.8 nm. If the same ionic strength of $MgCl_2$ was applied, the averaged hydrodynamic diameter of silica–high MW PDDA reduced to 235.8 nm, equivalent to 28.3% shrinkage of the layer thickness.

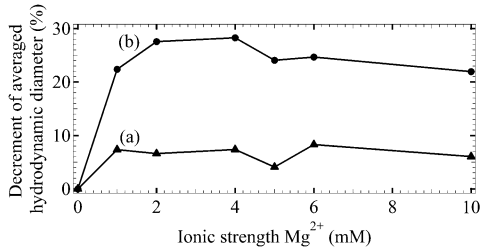

Figure 5. Averaged hydrodynamic diameter decrement of (a) silica–low MW PDDA (▲) and (b) silica–high MW PDDA (●) by varying the ionic strength of $MgCl_2$ from 0 to 10 mM.

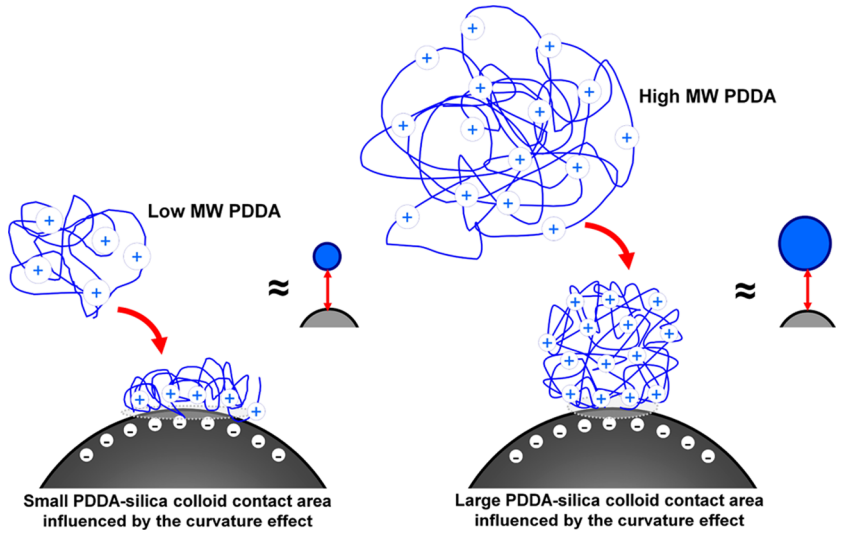

Figure 6. Schematic diagram for the interaction of low and high MW PDDA with the silica colloid of the same dimension. The radius of curvature effect is more pronounced for high MW PDDA.

Apparently, PDDA-coated silica colloid experienced a salting out effect when subjected to an electrolyte solution composed of a divalent salt.[51−53] This shrinkage is resulting from the interaction between divalent salt ions and the conformation chains of the adsorbed polyelectrolyte on silica colloids surface.[54] Strong electrostatic repulsion initially existed between polyelectrolyte segments,[55] and thus, polyelectrolyte tends to swell into extended conformation.[56,57] By replacing pure Milli-Q water with divalent electrolyte, the intersegment electrostatic repulsion was screened by the free ionic species that exist.[58] Therefore, the addition of electrolyte has suppressed the effective electrostatic repulsion between polyelectrolyte segments, leading to the collapse of polyelectrolyte chains onto the silica surface.[57] Divalent counterions were employed in this study instead of monovalent counterions due to the greater affinity of divalent ions to form a complex between two neighboring charged monomers and to precipitate the polyelectrolyte.[59]

From Figure 5, at the same ionic strength level, the decrement of averaged hydrodynamic diameter for silica−PDDA was higher when high MW PDDA was used as binding agent. This sharp contrast was ascribed to the different molecular weight of polyelectrolyte that was adsorbed on the silica colloid surface. From Table 1, the hydrodynamic diameter of high MW PDDA at 193.5 nm is almost double the size of low MW PDDA, with diameter at 96.7 nm. Hence, the local interfacial contact area between low MW PDDA molecule and silica colloid resembles a slight flatter surface compared to that of high MW PDDA and silica colloid, mainly due to the size mismatch (see Figure 6). Under this scenario, the overall contact area between silica is considered greater for low MW PDDA compared to high MW PDDA. This phenomenon is in consistent with many other works that revealed that curvature mismatch between two entities with different size would influence the interacting area between them, and this effect is more pronounced on the nanoscale.[41] Our observation in which the layer thickness is dependent on polyelectrolyte molecular weight is opposed to the existing literature.[60,61] On top of the contribution of size mismatch between the silica colloid and PDDA molecules discussed previously, the high concentration of PDDA molecules we used should also play an important role in causing these contradicting results.[62] Besides, smaller likewise surface curvature gave weaker interaction, and thus, high MW PDDA appeared in a more flexi-extended conformation on the silica surface.[63] This consideration is in accordance with the study of polymer at an interface reported by Fleer.[64] Within the context of this argument, the configuration of adsorbed polyelectrolyte on the particle surface can best be described in terms of trains, loops, and tails, which are determined by polyelectrolyte properties and adsorption conditions, such as polyelectrolyte molecular weight.[64,65] These theoretical findings can thus be implemented to explain our current observations. Under this scenario, low MW PDDA was most probably reoriented in a relatively flat and compact configuration upon adsorption to the silica surface, as mandated for effective charge inversion.[64] On the other hand, the layer thickness of high MW PDDA suffered a higher degree of suppression during the addition of divalent salt. This situation illustrated that high MW PDDA adsorbed on silica colloids surface may be more energetically favorable, where more ramified structures of trains, loops, and tails conformations existed accompanied by extra interstitial space for greater collapse to occur.[64]

The response of adsorbed PDDA layer toward the ionic strength increment of the background medium was also studied using QCM-D to provide complementary evidence to the DLS measurement (see Figure 7). A drastic decrease in dissipation shift was observed by changing the working solution from Milli-

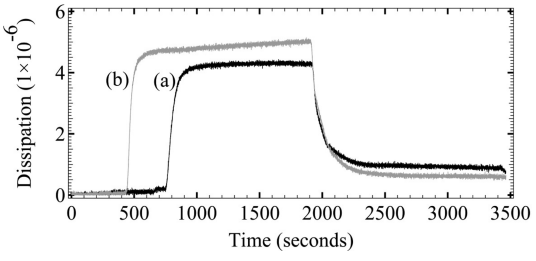

Figure 7. Changes in dissipation as a function of time of (a) low MW PDDA (black line) and (b) high MW PDDA (gray line) on silica-coated quartz crystal by changing the background medium from Milli-Q water to 10 mM $MgCl_2$ solution at 1800 s.

dx.doi.org/10.1021/am5050949 | ACS Appl. Mater. Interfaces 2014, 6, 16508−16518

Q water to 10 mM $MgCl_2$, indicating that the adsorbed polyelectrolyte collapsed into a more compact structure. This observation is consistent with our previous DLS result and has also been reported by others.[66] On top of that, considerably more pronounced decrement of dissipation shift was detected for the high MW PDDA layer compared to the low MW PDDA layer upon the introduction of 10 mM $MgCl_2$ solution. This conspicuous difference was confidently interpreted as a sign of the higher degree of openness exhibited by the adsorbed high MW PDDA, corresponding to the greater extent of the collapsing layer. The more extended conformation adopted by adsorbed high MW PDDA can essentially be rationalized as the contribution of the enhanced steric barrier and electrostatic repulsion exhibited in longer polyelectrolyte chains stimulating the polyelectrolyte chains to protrude outward.[49] The point we want to stress here is that this circumstance became of particular significance and a remarkable principle for the subsequent immobilization of IONPs into the PDDA shell.

Conversely, more extended/fuzzier-structured magnetic core–shell nanoparticles constructed with high MW PDDA gave a branched IONPs distribution and observable scattered IONPs aggregates on the outer surface of silica colloid. In order to check the benefit of having such a distinctively different structure for practical usages, we further proceed with probing its pollutant removal capability by taking amoxicillin as our modeled system.

3.3. Amoxicillin (AMX) Removal Test. Figure 8 shows that it is possible to use PDDA-coated silica colloid alone to remove 4.9% (low MW PDDA) and 11.8% (high MW PDDA) of AMX. From Table 1, the effective surface charge of the silica colloid after the attachment of the PDDA layer is quite positive and registered ζ-potential values of +51.0 and +56.6 mV for particles coated with low and high MW PDDA, respectively. On the other hand, the AMX molecules were detected to have a very minor ζ-potential value at +0.587 mV under our working conditions. This result was in agreement with the study done by Goddard and co-workers reporting that AMX existed as a zwitterion with negligible positive charge approaching zero between pH 3 and 6.[67] In fact, AMX contained three ionizable groups identified as carboxylic acid (pK_a = 2.68), amine (pK_a = 7.49), and phenolic hydroxyl (pK_a = 9.63), and hence, AMX can always existed in ionized form for the entire pH range from 1 to 14.[67] In this study, we did not carry out any pH adjustment and the reaction mixture was deionized water within the pH range of 6.3–6.8, which is higher than the pK_a of the carboxyl group but lower than that of the amine moiety. Thus, the carboxyl group of AMX presented as $-COO^-$ and amine group was in the form of $-NH_3^+$. For the case of silica–PDDA, the primary interaction was interpreted to occur between the positively charged polyelectrolyte segments and the carboxyl functional groups of AMX, which triggers the minor adsorption of AMX toward the polyelectrolyte matrix, leading to a removal efficiency at 4.9% for low MW PDDA and 11.8% for high MW PDDA, respectively.

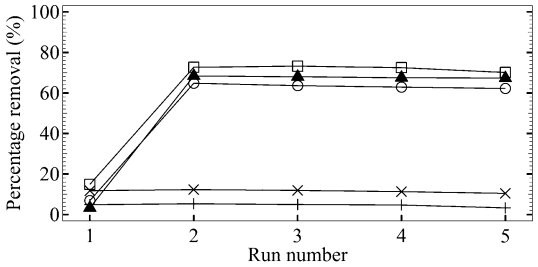

Figure 8. Amoxicillin antibiotic removal by IONPs (▲), silica–low MW PDDA (+), silica–high MW PDDA (×), silica–low MW PDDA–IONPs (○), and silica–high MW PDDA–IONPs (□) in the experiment without H_2O_2 (1st cycle) and in the presence of H_2O_2 (recycling run 2–5), with all particle concentrations of 0.01 g/mL.

After the attachment of IONPs, but without the addition of H_2O_2 as electron donor (with minimum catalytic degradation), both silica–low MW PDDA–IONPs and silica–high MW PDDA–IONPs nanocomposite managed to achieve 6.9% and 14.9% of AMX removal, respectively. There is a minor but observable increment of 2.0% (low MW PDDA) and 3.1% (high MW PDDA) after the introduction of IONPs into silica–PDDA. This increment efficiency is comparable to the AMX removal of 3.3% achieved by bare IONPs. The low AMX removal by IONPs at 3.3% was believed to be contributed by the weak electrostatic interaction between the negatively charged IONPs (−16.4 mV) and positively charged AMX (+0.578 mV) (see Table 1). Under this condition, it is very likely that the negatively charged IONPs, which have been embedded on and/or within the PDDA layer of silica–PDDA, contribute to the better performance in AMX removal. The minor AMX removal enhancement was attributed to the complex interplay between localized anionic IONPs with the amine group of AMX and the extended positively charged polyelectrolyte with the carboxyl group of AMX. This comparison between silica–PDDA and silica–PDDA–IONPs without the addition of H_2O_2 has verified the importance of localized charge(s) in AMX removal, regardless the overall charge of the entire nanostructure. By further recycling these particles for another round of AMX removal, but this time in the presence of H_2O_2, the AMX removal efficiency achieved by silica–low MW PDDA and silica–high MW PDDA was 5.3% and 12.3%, respectively. Under this scenario, AMX removal efficiency did not altered much for silica–PDDA (without IONPs) in either case of low or high MW PDDA. In contrast, for the case of bare IONPs, silica–low MW PDDA–IONPs, and silica–high MW PDDA–IONPs, we recorded a significant boost in term of AMX removal efficiency at 68.4%, 64.8%, and 72.7%, respectively. These two sets of experiment were conducted to exclude the contribution of an adsorption process due to a counterion condensation effect. Furthermore, we have also excluded the charge density difference between the low- and high MW PDDA in removing AMX, since the charged sites on the polyelectrolyte matrix are pretty much saturated during the first removal cycle of AMX. Indirectly, the further removal of AMX in the presence of H_2O_2, comparing to the condition without H_2O_2, was dominated by the occurrence of an advanced oxidation process.[68] With this observation, it is logical to believe that high MW PDDA, which forms a more extended polyelectrolyte layer, plays a dominant role in AMX removal. The underlying mechanism related to this hypothesis can be addressed by applying the concept presented in the previous section. In short, the availability of a more conformational structure has indirectly eased the migration of AMX molecules from surrounding media to reach the IONP surface embedded within the PDDA matrix. This in turn enhanced the catalytic degradation of AMX as the modeled pollutant. It is worth it to mention that although the removal efficiency achieved by bare IONPs was higher than that of silica–low MW PDDA–IONPs (but lower than that of silica–high MW PDDA–IONPs), it took up to 1 day to fully recover

all of them from the suspension through magnetic collection (see Figure S3 in Supporting Information). The long separation time with slow collection kinetic makes the sole use of IONPs as catalytic material for water treatment purpose less attractive.[69] In order to verify the preservation of the catalytic function, the recyclability of all synthesized nanoparticles, namely, IONPs, silica–low MW PDDA, silica–high MW PDDA, silica–low MW PDDA–IONPs, and silica–high MW PDDA–IONPs, was assessed by subjecting them to three more cycles of AMX removal. It was observed that the catalytic silica–PDDA–IONPs and IONPs retained high AMX removal efficiency after a total of four consecutive runs (including the initial run) in catalytic AMX removal experiments, despite a slight decrease from each run (see Figure 8). To study the possible leaching of IONPs from nanocomposite into the solution, which may responsible for the decrement of AMX removal efficiency, the iron content was measured in the supernatant after the recycling process. From this measurement, only around 8.0×10^{-3}% of iron content was detected at the end of the entire recycling process, which confirmed the excellent stability of the nanocomposite (see Table S2 in the Supporting Information). From this observation, we have proven that the ultimate structure of the synthesized nanocomposite is robust enough to survive through the harsh cycle of the Fenton reaction without experiencing significant dissolution of IONPs due to destabilization of the polyelectrolyte layer. Therefore, the moderate decrement of catalytic activity was believed to originate from the contamination of nanocomposite and IONPs influenced by some of the organic intermediates that remain strongly adsorbed on the IONPs surface.[69]

4. CONCLUSION

Silica and iron oxide core–shell nanoparticles with extended shell structure are synthesized by using polyelectrolyte with different molecular weight as binding agent. PDDA with high molecular weight is a better candidate for the construction of a more extended, open polymeric matrix that can be used to incorporate IONPs into the open shell. Moreover, it has also been demonstrated that a change in polyelectrolyte molecular weight could dramatically altered the distribution of immobilized IONPs on the as-synthesized silica core–IONP shell nanocomposite. This feature is mainly influenced by (1) conformation of the adsorbed PDDA layer, where high MW PDDA tends to form a more extended, loosely packed layer compared to low MW PDDA, and (2) size mismatch between the PDDA and silica colloid. DLS and QCM-D measurements are employed to determine the thickness and viscoelastic property of the PDDA layer formed. By using amoxicillin as the model system, we tested the pollutant removal capability of this core–shell nanomaterial from an aqueous environment. Core–shell nanoparticles with high MW PDDA as binding agent give better AMX removal efficiency mainly due to the highly extended PDDA structure formed, which imposes less mass transfer resistance for the migration of AMX macromolecules. Besides, the overall charge of the core–shell nanoparticles formed is less significant compared to the localized charge in determining the removal efficiency of AMX. Understanding the role of polyelectrolyte on influencing the surface structure of nanocomposite formed offers a new opportunity to design nanomaterials with fine-tuned functionality for water treatment purposes.

■ ASSOCIATED CONTENT

Supporting Information

Colloidal stability profiles and real-time magnetophoretic separation rates of IONPs, silica–low MW PDDA–IONPs, and silica–high MW PDDA–IONPs; temporal evolution of suspension opacity for bare IONPs and silica–PDDA–IONPs; diameters of nanoparticles determined by TEM and DLS; and the total iron content leached out from nanocomposite after five consecutive runs of AMX removal (Figures S1–S3 and Tables S1 and S2). This material is available free of charge via the Internet at http://pubs.acs.org.

■ AUTHOR INFORMATION

Corresponding Author

*E-mail: chjitkangl@usm.my. Tel: +60-4-599-6423. Fax: +60-4-599-1013.

Notes

The authors declare no competing financial interest.

■ ACKNOWLEDGMENTS

This project is financially supported by RU grant from Universiti Sains Malaysia (Grant No. 1001/PJKIMIA/811219), FRGS grant from MOHE (Grant No. 203/PJKIMIA/6071269), and International Foundation for Science (IFS) (Grant No. 304/PJKIMIA/6050232). All authors are affiliated with the Membrane Science and Technology Cluster of USM.

■ REFERENCES

(1) Fernández-Ibáñez, P.; Blanco, J.; Malato, S.; Nieves, F. J. d. l. Application of the Colloidal Stability of TiO_2 Particles for Recovery and Reuse in Solar Photocatalysis. *Water Res.* **2003**, *37*, 3180–3188.

(2) Chowdhury, I.; Duch, M. C.; Mansukhani, N. D.; Hersam, M. C.; Bouchard, D. Colloidal Properties and Stability of Graphene Oxide Nanomaterials in the Aquatic Environment. *Environ. Sci. Technol.* **2013**, *47*, 6288–6296.

(3) Decher, G. Fuzzy Nanoassemblies: Toward Layered Polymeric Multicomposites. *Science* **1997**, *277*, 1232–1237.

(4) Grzybowski, B. A.; Wilmer, C. E.; Kim, J.; Browne, K. P.; Bishop, K. J. M. Self-Assembly: From Crystals to Cells. *Soft Matter* **2009**, *5*, 1110–1128.

(5) Kotov, N. A.; Dekany, I.; Fendler, J. H. Layer-by-Layer Self-Assembly of Polyelectrolyte–Semiconductor Nanoparticle Composite Films. *J. Phys. Chem.* **1995**, *99*, 13065–13069.

(6) Kovtyukhova, N. I.; Ollivier, P. J.; Martin, B. R.; Mallouk, T. E.; Chizhik, S. A.; Buzaneva, E. V.; Gorchinskiy, A. D. Layer-by-Layer Assembly of Ultrathin Composite Films from Micron-Sized Graphite Oxide Sheets and Polycations. *Chem. Mater.* **1999**, *11*, 771–778.

(7) Correa-Duarte, M. A.; Kosiorek, A.; Kandulski, W.; Giersig, M.; Liz-Marzán, L. M. Layer-by-Layer Assembly of Multiwall Carbon Nanotubes on Spherical Colloids. *Chem. Mater.* **2005**, *17*, 3268–3272.

(8) Grzelczak, M.; Vermant, J.; Furst, E. M.; Liz-Marzán, L. M. Directed Self-Assembly of Nanoparticles. *ACS Nano* **2010**, *4*, 3591–3605.

(9) Yeap, S. P.; Toh, P. Y.; Ahmad, A. L.; Low, S. C.; Majetich, S. A.; Lim, J. Colloidal Stability and Magnetophoresis of Gold-Coated Iron Oxide Nanorods in Biological Media. *J. Phys. Chem. C* **2012**, *116*, 22561–22569.

(10) Berret, J.-F.; Schonbeck, N.; Gazeau, F.; El Kharrat, D.; Sandre, O.; Vacher, A.; Airiau, M. Controlled Clustering of Superparamagnetic Nanoparticles Using Block Copolymers: Design of New Contrast Agents for Magnetic Resonance Imaging. *J. Am. Chem. Soc.* **2006**, *128*, 1755–1761.

(11) Liang, Z.; Susha, A.; Caruso, F. Gold Nanoparticle-Based Core–Shell and Hollow Spheres and Ordered Assemblies Thereof. *Chem. Mater.* **2003**, *15*, 3176–3183.
(12) Zhang, L.; Qiao, S. Z.; Jin, Y. G.; Chen, Z. G.; Gu, H. C.; Lu, G. Q. Magnetic Hollow Spheres of Periodic Mesoporous Organosilica and Fe_3O_4 Nanocrystals: Fabrication and Structure Control. *Adv. Mater.* **2008**, *20*, 805–809.
(13) Phenrat, T.; Saleh, N.; Sirk, K.; Tilton, R. D.; Lowry, G. V. Aggregation and Sedimentation of Aqueous Nanoscale Zerovalent Iron Dispersions. *Environ. Sci. Technol.* **2006**, *41*, 284–290.
(14) Auffan, M.; Rose, J.; Bottero, J.-Y.; Lowry, G. V.; Jolivet, J.-P.; Wiesner, M. R. Towards a Definition of Inorganic Nanoparticles from an Environmental, Health and Safety Perspective. *Nat. Nano* **2009**, *4*, 634–641.
(15) Nowack, B.; Bucheli, T. D. Occurrence, Behavior and Effects of Nanoparticles in the Environment. *Environ. Pollut.* **2007**, *150*, 5–22.
(16) Benelmekki, M.; Caparros, C.; Montras, A.; Gonçalves, R.; Lanceros-Mendez, S.; Martinez, L. M. Horizontal Low Gradient Magnetophoresis Behaviour of Iron Oxide Nanoclusters at the Different Steps of the Synthesis Route. *J. Nanopart. Res.* **2011**, *13*, 3199–3206.
(17) Faraudo, J.; Camacho, J. Cooperative Magnetophoresis of Superparamagnetic Colloids: Theoretical Aspects. *Colloid Polym. Sci.* **2010**, *288*, 207–215.
(18) Che, H. X.; Yeap, S. P.; Ahmad, A. L.; Lim, J. Layer-by-Layer Assembly of Iron Oxide Magnetic Nanoparticles Decorated Silica Colloid for Water Remediation. *Chem. Eng. J.* **2014**, *243*, 68–78.
(19) Karumanchi, R. S. M. S.; Doddamane, S. N.; Sampangi, C.; Todd, P. W. Field-Assisted Extraction of Cells, Particles and Macromolecules. *Trends Biotechnol.* **2002**, *20*, 72–78.
(20) Podsiadlo, P.; Choi, S.-Y.; Shim, B.; Lee, J.; Cuddihy, M.; Kotov, N. A. Molecularly Engineered Nanocomposites: Layer-by-Layer Assembly of Cellulose Nanocrystals. *Biomacromolecules* **2005**, *6*, 2914–2918.
(21) Ma, R.; Sasaki, T.; Bando, Y. Layer-by-Layer Assembled Multilayer Films of Titanate Nanotubes, Ag- or Au-Loaded Nanotubes, and Nanotubes/Nanosheets with Polycations. *J. Am. Chem. Soc.* **2004**, *126*, 10382–10388.
(22) Olek, M.; Ostrander, J.; Jurga, S.; Möhwald, H.; Kotov, N.; Kempa, K.; Giersig, M. Layer-by-Layer Assembled Composites from Multiwall Carbon Nanotubes with Different Morphologies. *Nano Lett.* **2004**, *4*, 1889–1895.
(23) Zhao, X.; Lv, L.; Pan, B.; Zhang, W.; Zhang, S.; Zhang, Q. Polymer-Supported Nanocomposites for Environmental Application: A Review. *Chem. Eng. J.* **2011**, *170*, 381–394.
(24) Pan, B.; Xie, Y.; Zhang, S.; Lv, L.; Zhang, W. Visible Light Photocatalytic Degradation of RhB by Polymer–CdS Nanocomposites: Role of the Host Functional Groups. *ACS Appl. Mater. Interfaces* **2012**, *4*, 3938–3943.
(25) De Baere, S.; De Backer, P. Quantitative Determination of Amoxicillin in Animal Feed Using Liquid Chromatography with Tandem Mass Spectrometric Detection. *Anal. Chim. Acta* **2007**, *586*, 319–325.
(26) Aksu, Z.; Tunç, Ö. Application of Biosorption for Penicillin G Removal: Comparison with Activated Carbon. *Process Biochem.* **2005**, *40*, 831–847.
(27) Pan, X.; Deng, C.; Zhang, D.; Wang, J.; Mu, G.; Chen, Y. Toxic Effects of Amoxicillin on the Photosystem II of *Synechocystis* Sp. Characterized by a Variety of in Vivo Chlorophyll Fluorescence Tests. *Aquat. Toxicol.* **2008**, *89*, 207–213.
(28) Nozawa, K.; Gailhanou, H.; Raison, L.; Panizza, P.; Ushiki, H.; Sellier, E.; Delville, J. P.; Delville, M. H. Smart Control of Monodisperse Stöber Silica Particles: Effect of Reactant Addition Rate on Growth Process. *Langmuir* **2004**, *21*, 1516–1523.
(29) Zhu, Y.; Wu, Q. Synthesis of Magnetite Nanoparticles by Precipitation with Forced Mixing. *J. Nanopart. Res.* **1999**, *1*, 393–396.
(30) Louie, S. M.; Phenrat, T.; Small, M. J.; Tilton, R. D.; Lowry, G. V. Parameter Identifiability in Application of Soft Particle Electrokinetic Theory to Determine Polymer and Polyelectrolyte Coating Thicknesses on Colloids. *Langmuir* **2012**, *28*, 10334–10347.
(31) Gittings, M. R.; Saville, D. A. The Determination of Hydrodynamic Size and Zeta Potential from Electrophoretic Mobility and Light Scattering Measurements. *Colloids Surf., A* **1998**, *141*, 111–117.
(32) Lim, J.; Tilton, R. D.; Eggeman, A.; Majetich, S. A. Design and Synthesis of Plasmonic Magnetic Nanoparticles. *J. Magn. Magn. Mater.* **2007**, *311*, 78–83.
(33) Lim, J.; Yeap, S. P.; Low, S. C. Challenges Associated to Magnetic Separation of Nanomaterials at Low Field Gradient. *Sep. Sci. Technol.* **2014**, *123*, 171–174.
(34) Putra, E. K.; Pranowo, R.; Sunarso, J.; Indraswati, N.; Ismadji, S. Performance of Activated Carbon and Bentonite for Adsorption of Amoxicillin from Wastewater: Mechanisms, Isotherms and Kinetics. *Water Res.* **2009**, *43*, 2419–2430.
(35) Larsson, C.; Rodahl, M.; Höök, F. Characterization of DNA Immobilization and Subsequent Hybridization on a 2D Arrangement of Streptavidin on a Biotin-Modified Lipid Bilayer Supported on SiO_2. *Anal. Chem.* **2003**, *75*, 5080–5087.
(36) Höök, F.; Kasemo, B.; Nylander, T.; Fant, C.; Sott, K.; Elwing, H. Variations in Coupled Water, Viscoelastic Properties, and Film Thickness of a Mefp-1 Protein Film During Adsorption and Cross-Linking: A Quartz Crystal Microbalance with Dissipation Monitoring, Ellipsometry, and Surface Plasmon Resonance Study. *Anal. Chem.* **2001**, *73*, 5796–5804.
(37) Ayodele, O. B.; Lim, J. K.; Hameed, B. H. Pillared Montmorillonite Supported Ferric Oxalate as Heterogeneous Photo-Fenton Catalyst for Degradation of Amoxicillin. *Appl. Catal., A* **2012**, *413–414*, 301–309.
(38) Trovó, A. G.; Pupo Nogueira, R. F.; Agüera, A.; Fernandez-Alba, A. R.; Malato, S. Degradation of the Antibiotic Amoxicillin by Photo-Fenton Process—Chemical and Toxicological Assessment. *Water Res.* **2011**, *45*, 1394–1402.
(39) Ghauch, A.; Tuqan, A.; Assi, H. A. Antibiotic Removal from Water: Elimination of Amoxicillin and Ampicillin by Microscale and Nanoscale Iron Particles. *Environ. Pollut.* **2009**, *157*, 1626–1635.
(40) Nägele, E.; Moritz, R. Structure Elucidation of Degradation Products of the Antibiotic Amoxicillin with Ion Trap MS^n and Accurate Mass Determination by ESI TOF. *J. Am. Soc. Mass. Spectrom.* **2005**, *16*, 1670–1676.
(41) Lundqvist, M.; Sethson, I.; Jonsson, B.-H. Protein Adsorption onto Silica Nanoparticles: Conformational Changes Depend on the Particles' Curvature and the Protein Stability. *Langmuir* **2004**, *20*, 10639–10647.
(42) Amirkhani, M.; Volden, S.; Zhu, K.; Glomm, W. R.; Nyström, B. Adsorption of Cellulose Derivatives on Flat Gold Surfaces and on Spherical Gold Particles. *J. Colloid Interface Sci.* **2008**, *328*, 20–28.
(43) Caruso, F.; Lichtenfeld, H.; Donath, E.; Möhwald, H. Investigation of Electrostatic Interactions in Polyelectrolyte Multilayer Films: Binding of Anionic Fluorescent Probes to Layers Assembled onto Colloids. *Macromolecules* **1999**, *32*, 2317–2328.
(44) Jans, H.; Liu, X.; Austin, L.; Maes, G.; Huo, Q. Dynamic Light Scattering as a Powerful Tool for Gold Nanoparticle Bioconjugation and Biomolecular Binding Studies. *Anal. Chem.* **2009**, *81*, 9425–9432.
(45) Otzen, D. E.; Oliveberg, M.; Höök, F. Adsorption of a Small Protein to a Methyl-Terminated Hydrophobic Surfaces: Effect of Protein-Folding Thermodynamics and Kinetics. *Colloids Surf., B* **2003**, *29*, 67–73.
(46) Su, X.; Zong, Y.; Richter, R.; Knoll, W. Enzyme Immobilization on Poly(ethylene-*co*-acrylic acid) Films Studied by Quartz Crystal Microbalance with Dissipation Monitoring. *J. Colloid Interface Sci.* **2005**, *287*, 35–42.
(47) Höök, F.; Rodahl, M.; Brzezinski, P.; Kasemo, B. Energy Dissipation Kinetics for Protein and Antibody–Antigen Adsorption under Shear Oscillation on a Quartz Crystal Microbalance. *Langmuir* **1998**, *14*, 729–734.
(48) Binnig, G.; Quate, C. F.; Gerber, C. Atomic Force Microscope. *Phys. Rev. Lett.* **1986**, *56*, 930–933.

(49) Porus, M.; Maroni, P.; Borkovec, M. Response of Adsorbed Polyelectrolyte Monolayers to Changes in Solution Composition. *Langmuir* **2012**, *28*, 17506−17516.
(50) Stevens, M. J.; Plimpton, S. J. The Effect of Added Salt on Polyelectrolyte Structure. *Eur. Phys. J. B* **1998**, *2*, 341−345.
(51) Miyamoto, S.; Imai, N. The Release of Monovalent Counterions by Addition of Divalent Counterions in Coulombic Interaction System. *Biophys. Chem.* **1980**, *11*, 345−352.
(52) Michaeli, I. Ion Binding and the Formation of Insoluble Polymethacrylic Salts. *J. Polym. Sci.* **1960**, *48*, 291−299.
(53) Ikegami, A.; Imai, N. Precipitation of Polyelectrolytes by Salts. *J. Polym. Sci.* **1962**, *56*, 133−152.
(54) Wang, Y.; Dubin, P. L. Protein Binding on Polyelectrolyte-Treated Glass: Effect of Structure of Adsorbed Polyelectrolyte. *J. Chromatogr. A* **1998**, *808*, 61−70.
(55) Van der Schee, H. A.; Lyklema, J. A Lattice Theory of Polyelectrolyte Adsorption. *J. Phys. Chem.* **1984**, *88*, 6661−6667.
(56) Böhme, U.; Scheler, U. Hydrodynamic Size and Electrophoretic Mobility of Poly(styrene sulfonate) Versus Molecular Weight. *Macromol. Chem. Phys.* **2007**, *208*, 2254−2257.
(57) Chremos, A.; Glynos, E.; Koutsos, V.; Camp, P. J. Adsorption and Self-Assembly of Linear Polymers on Surfaces: A Computer Simulation Study. *Soft Matter* **2009**, *5*, 637−645.
(58) Yeap, S. P.; Ahmad, A. L.; Ooi, B. S.; Lim, J. Electrosteric Stabilization and Its Role in Cooperative Magnetophoresis of Colloidal Magnetic Nanoparticles. *Langmuir* **2012**, *28*, 14878−14891.
(59) Sabbagh, I.; Delsanti, M. Solubility of Highly Charged Anionic Polyelectrolytes in Presence of Multivalent Cations: Specific Interaction Effect. *Eur. Phys. J. E: Soft Matter Biol. Phys.* **2000**, *1*, 75−86.
(60) Seyrek, E.; Hierrezuelo, J.; Sadeghpour, A.; Szilagyi, I.; Borkovec, M. Molecular Mass Dependence of Adsorbed Amount and Hydrodynamic Thickness of Polyelectrolyte Layers. *Phys. Chem. Chem. Phys.* **2011**, *13*, 12716−12719.
(61) Kong, C. Y.; Muthukumar, M. Monte Carlo Study of Adsorption of a Polyelectrolyte onto Charged Surfaces. *J. Chem. Phys.* **1998**, *109*, 1522−1527.
(62) Oedberg, L.; Sandberg, S.; Welin-Klintstroem, S.; Arwin, H. Thickness of Adsorbed Layers of High Molecular Weight Polyelectrolytes Studied by Ellipsometry. *Langmuir* **1995**, *11*, 2621−2625.
(63) Garg, A.; Heflin, J. R.; Gibson, H. W.; Davis, R. M. Study of Film Structure and Adsorption Kinetics of Polyelectrolyte Multilayer Films: Effect of pH and Polymer Concentration. *Langmuir* **2008**, *24*, 10887−10894.
(64) Fleer, G. J. Polymers at Interfaces and in Colloidal Dispersions. *Adv. Colloid Interface Sci.* **2010**, *159*, 99−116.
(65) Fleer, G. J.; Scheutjens, J. M. H. M.; Stuart, M. A. C. Theoretical Progress in Polymer Adsorption, Steric Stabilization and Flocculation. *Colloids Surf.* **1988**, *31*, 1−29.
(66) Notley, S. M.; Biggs, S.; Craig, V. S. J.; Wagberg, L. Adsorbed Layer Structure of a Weak Polyelectrolyte Studied by Colloidal Probe Microscopy and QCM-D as a Function of pH and Ionic Strength. *Phys. Chem. Chem. Phys.* **2004**, *6*, 2379−2386.
(67) Goddard, A. F.; Jessa, M. J.; Barrett, D. A.; Shaw, P. N.; Idstrom, J. P.; Cederberg, C.; Spiller, R. C. Effect of Omeprazole on the Distribution of Metronidazole, Amoxicillin, and Clarithromycin in Human Gastric Juice. *Gastroenterology* **1996**, *111*, 358−367.
(68) Elmolla, E.; Chaudhuri, M. Optimization of Fenton Process for Treatment of Amoxicillin, Ampicillin and Cloxacillin Antibiotics in Aqueous Solution. *J. Hazard. Mater.* **2009**, *170*, 666−672.
(69) Ferroudj, N.; Nzimoto, J.; Davidson, A.; Talbot, D.; Briot, E.; Dupuis, V.; Bée, A.; Medjram, M. S.; Abramson, S. Maghemite Nanoparticles and Maghemite/Silica Nanocomposite Microspheres as Magnetic Fenton Catalysts for the Removal of Water Pollutants. *Appl. Catal., B* **2013**, *136−137*, 9−18.